

# Characterization of the static behavior of micromirrors under the effect of capillary force, an analytical approach

Proc IMechE Part C:  
*J Mechanical Engineering Science*  
226(9) 2361–2372  
© IMechE 2012  
Reprints and permissions:  
sagepub.co.uk/journalsPermissions.nav  
DOI: 10.1177/0954406211433112  
pic.sagepub.com



**Hamid Moeenfarid, Ali Darvishian, Hassan Zohoor and Mohammad Taghi Ahmadian**

## Abstract

In this article, the static behavior of micromirrors under the effect of capillary force is studied. The dimensionless equations governing the static behavior and the pull-in state of the micromirror under capillary force are obtained, and the effects of different geometrical parameters on the pull-in angle of micromirrors are investigated. The static behavior of micromirrors is studied both numerically and analytically using the homotopy perturbation method. It is observed that with increasing the instability number defined in this article, the rotation angle of the micromirror is increased and suddenly the pull-in occurs. The results of the presented model are then verified by comparing them with the results of finite element simulations performed in the commercial finite element model software ANSYS. The agreement between the results of finite element model and those of the proposed analytical model shows that homotopy perturbation method can be used as a fast and accurate tool for predicting mirror's behavior under capillary force.

## Keywords

Micromirror, capillary force, pull-in instability, homotopy perturbation method, finite element simulation

Date received: 5 June 2011; accepted: 23 November 2011

## Introduction

Microelectromechanical systems (MEMS) are being developed for a wide spectrum of applications in various aspects of life.<sup>1</sup> These devices make the systems faster, more reliable, cheaper, and capable of incorporating more complex functions.<sup>2</sup> Successful MEMS devices rely not only on well-developed fabrication technologies, but also on the knowledge of device behavior.<sup>3</sup>

The fact that MEMS devices play important roles in optical systems caused the development of a new class of systems called micro-opto-electro-mechanical systems (MOEMS). MOEMS include a wide variety of devices including digital micromirror devices,<sup>4</sup> optical switches,<sup>5</sup> microscanning mirrors,<sup>6</sup> optical cross-connects,<sup>7,8</sup> etc. Torsional actuators play an important role in MOEMS.<sup>9</sup> Many research studies have been done on torsional micro-actuators. For example, Degani et al.<sup>10</sup> presented a novel displacement iteration pull-in extraction scheme for the problem of electrostatic torsion micro-actuators. They<sup>10</sup> showed that their presented method converges 100 times faster

than the voltage iteration scheme. Xiao and Farmer<sup>11</sup> investigated the stability of single-crystal silicon, rectangular, electrostatic torsion actuators in a variety of ambients and configurations. Zhang et al.<sup>12</sup> described the static characteristics of an electrostatically actuated torsional micromirror based on parallel plate capacitor model. They extensively studied the snap-down phenomenon in micromirrors. They used numerical approach for their simulations. Huang et al.<sup>9</sup> presented a general theoretical model using the coupling effect between the torsion and bending in electrostatic torsional actuators. They also presented experiments to verify their model which was numerically solved.

The influence of van der Waals (vdW) and casimir forces on the behavior of MEMS and

---

Center of Excellence in Design, Robotics and Automation, School of Mechanical Engineering, Sharif University of Technology, Iran

### Corresponding author:

Mohammad Taghi Ahmadian, Center of Excellence in Design, Robotics and Automation, School of Mechanical Engineering, Sharif University of Technology, Tehran, Iran.  
Email: ahmadian@mech.sharif.edu

nanoelectromechanical systems (NEMS) has also been extensively studied by many researchers.<sup>13–16</sup> Guo and Zhao<sup>15</sup> discussed the effect of vdW and casimir force on the torsional micro-actuators. Gusso and Delben<sup>16</sup> studied the influence of the casimir force on the silicon-based actuators. In addition to casimir and vdW forces, capillary force is one of the most important surface forces that play a crucial role in MEMS. Existence of a liquid bridge between two objects results in the formation of capillary force.<sup>17</sup> The existence of capillary force even in low relative humidity is experimentally observed.<sup>18</sup> Parallel plate MEMS actuators are conventionally fabricated by forming a layer of a plate or beam material on the top of a sacrificial layer and wet etching the sacrificial layer. So, the capillary force can be easily formed and if it is large enough, the microbeam or plate will collapse and adhere to the substrate. Hence, the investigation of the static deflection of micromirrors under capillary force seems to be essential.<sup>19</sup> Mastrangelo and Hsu<sup>20,21</sup> theoretically and experimentally studied the stability and adhesion of thin micromechanical structures under capillary force. Recently, the instability of torsional MEMS/NEMS actuators under capillary force was investigated by Guo et al.<sup>19</sup> Moeenfarid et al.<sup>22</sup> proposed an extended Kantorovich method to analyze static behavior of microplates under the effect of capillary force. In addition, the effects of capillary force on the static and dynamic behaviors of atomic force microscopes have been widely assessed,<sup>23–25</sup> but the static behavior of micromirrors under the effect of capillary force around their stable operative range has not yet been presented.

Perturbation methods have been used to analytically solve the nonlinear problems in MEMS. Younis and Nayfeh<sup>26</sup> investigated the response of a resonant microbeam to an electric actuation using the multiple-scale perturbation method. Abdel-Rahman and Nayfeh<sup>27</sup> used the same method to model secondary resonances in electrically actuated microbeams. Since perturbation methods are based upon the assumption that there is a small parameter in the equations, they have some limitations in problems without the involvement of small parameters. In order to overcome this limitation, a new perturbation-based method, namely homotopy perturbation method (HPM) was developed by He.<sup>28</sup> His new method takes full advantages of the traditional perturbation methods and homotopy techniques. Homotopy perturbation method has also been used for solving the nonlinear problems encountered in N/MEMS. For example, Moeenfarid et al.<sup>29</sup> used HPM to model the nonlinear vibration behavior of Timoshenko microbeams. Mojahedi et al.<sup>13</sup> applied the HPM method to simulate the static response of nano-switches to electrostatic actuation and

intermolecular surface forces. But so far, no analytic solution has been presented to model the behavior of micromirrors under capillary force.

In this article, the equations governing the static behavior of micromirrors are obtained using Newton's first law of motion and the effect of different design parameters on the pull-in angle of micromirrors is numerically studied. At the end, the static behavior of micromirrors is investigated both analytically and numerically using the presented model and also using FEM model presented in commercial FEM software, ANSYS. The analytical results will follow the numerical ones and can be used as a fast and accurate tool for predicting mirror's behavior under capillary force.

### Capillary torque on torsional micromirrors

The micromirror shown in Figure 1 is considered. As it is shown in this figure, the geometry of the liquid between the mirror and the substrate is considered to be known. It has to be noted that in practical situations, the geometry is more complex and the meniscus resulting from the surface tension will form along all sides of the mirror. In order to simplify the analysis, these menisci and also the corners that are formed at the

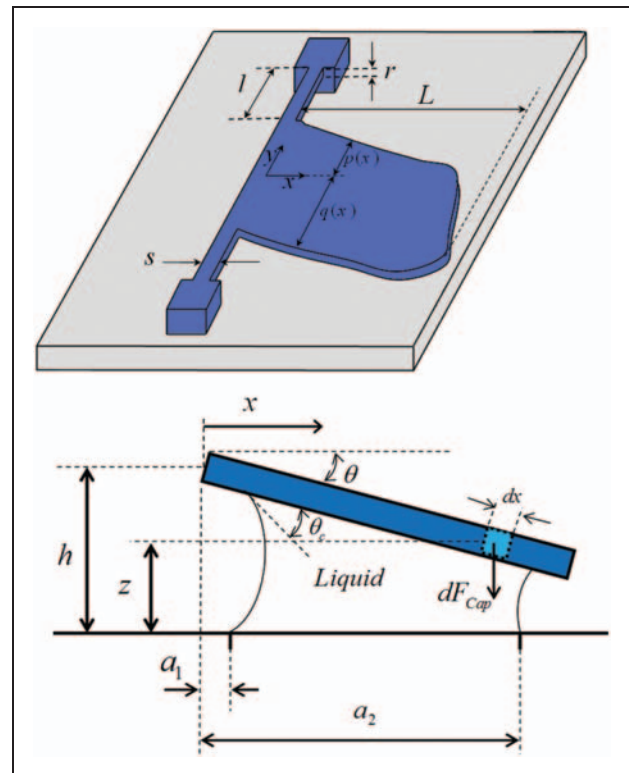


**Figure 1.** Schematic view of a micromirror under the effect of capillary force.

cross-sections of the two menisci have not been considered in the formulation.

In this sense, the capillary pressure on the micromirror can be computed as:<sup>19,20,22</sup>

$$P_{Cap} = \frac{2\gamma \cos \theta_c}{z} \quad (1)$$

where  $P_{Cap}$  is the capillary pressure,  $\gamma$  the surface energy of the liquid,  $\theta_c$  the contact angle between liquid and solid surfaces, and  $z$  the distance between the point with capillary pressure  $P_{Cap}$  and the underneath substrate. So, assuming that the torsion microbeams connected to the mirror do not undergo bending, the capillary torque applied to the micromirror would be as

$$M_{Cap} = 2\gamma \cos \theta_c \int_{a_1}^{a_2} \frac{x(p(x) - q(x))}{h - x \sin \theta} dx \quad (2)$$

where  $h$  is the initial distance between micromirror and the substrate,  $a_1$  and  $a_2$  some position parameters defining the start and end points of the liquid, as illustrated in Figure 1. Since the rotation angle in micromirrors is usually small,  $\sin \theta$  can be closely approximated by  $\theta$  and equation (2) can be restated as

$$M_{Cap} = 2\gamma \cos \theta_c \int_{a_1}^{a_2} \frac{x(p(x) - q(x))}{h - x\theta} dx \quad (3)$$

The mechanical restoring torque applied to the micromirror is obtained using the following relation

$$M_{Mech} = -K\theta \quad (4)$$

where<sup>9</sup>

$$K = \frac{2GI_p}{l} \quad (5)$$

In this equation,  $G$  is the shear modulus of the torsion beams,  $l$  the length of each torsion beam, and  $I_p$  the polar momentum of inertia of the rectangular cross-section expressed as:<sup>9</sup>

$$I_p = \frac{1}{3}rs^3 - \frac{64}{\pi^5}s^4 \sum_{n=1}^{\infty} \frac{1}{(2n-1)^5} \tanh \frac{(2n-1)\pi r}{2s} \quad (6)$$

where  $s$  and  $r$  are the width and length of the cross-section of the torsion beams, as illustrated in Figure 1. Using equations (5) and (6), equation (4) is simplified as follows.

$$M_{Mech} = -\frac{2GI_p}{l}\theta \quad (7)$$

At equilibrium point, the net torque applied to the micromirror is zero

$$M_{Cap} + M_{Mech} = 0 \quad (8)$$

Using equations (3) and (7), equation (8) is simplified to the following equation

$$\frac{2GI_p}{l}\theta - 2\gamma \cos \theta_c \int_{a_1}^{a_2} \frac{x(p(x) - q(x))}{h - x\theta} dx = 0 \quad (9)$$

By defining the dimensionless parameter  $\Theta = \theta/\theta_0$ , where  $\theta_0 = h/L$  is the maximum physically possible rotation angle of the mirror, equation (9) can be restated as follows

$$\mathfrak{S}(\Theta, \eta, \alpha, \beta) = \Theta - \eta.M(\alpha, \beta, \Theta) = 0 \quad (10)$$

where  $\mathfrak{S}$  is the equilibrium equation, and  $\eta$  and  $M(\alpha, \beta, \Theta)$  are defined as equations (11) and (12), respectively

$$\eta = \frac{2\gamma \cos \theta_c WL^3}{Kh^2} \quad (11)$$

$$M(\alpha, \beta, \Theta) = \frac{h}{WL^2} \int_{a_1}^{a_2} \frac{x(p(x) - q(x))}{h(1 - \frac{x}{L}\Theta)} dx \quad (12)$$

In these equations,  $\eta$  is called the instability number,  $W$  and  $L$  the width and length of the mirror, respectively, and  $\alpha$  and  $\beta$  some dimensionless parameters defined in equations (13) and (14), respectively

$$\alpha = \frac{a_1}{L} \quad (13)$$

$$\beta = \frac{a_2}{L} \quad (14)$$

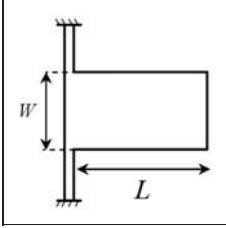
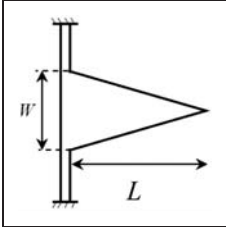
In Table 1, the functions  $p(x)$ ,  $q(x)$ , and  $M(\alpha, \beta, \Theta)$  for different designs of micromirrors have been presented.

Figure 2 shows the effect of changing the geometry of the mirror on the dimensionless capillary torque applied to it. It is observed that at equal values of  $\eta$ , the capillary torque applied to the rectangular mirrors is larger than that of triangular mirrors. This is due to the fact that in rectangular micromirrors, the capillary pressure is applied on a larger surface.

In Figure 3, the functions  $f(\Theta) = \Theta$  and  $g(\Theta) = \eta.M(\alpha, \beta, \Theta)$  have been plotted versus  $\Theta$  at various values of  $\eta$  for different types of designs of micromirrors presented in Table 1.

It is observed that at low values of  $\eta$ , there exist two roots for equation (10), where the smaller one is the stable equilibrium point and the larger one the unstable

**Table 1.** The functions  $p(x)$ ,  $q(x)$ , and  $M(\alpha, \beta, \Theta)$  for different designs of micromirrors.

Shape	Drawing	$p(x)$	$q(x)$	$M(\alpha, \beta, \Theta)$
Rectangular		$\frac{W}{2}$	$-\frac{W}{2}$	$\left(\frac{\alpha - \beta}{\Theta} - \frac{1}{\Theta^2} \ln\left(\frac{1 - \beta\Theta}{1 - \alpha\Theta}\right)\right)$
Triangular		$\frac{W}{2} - \frac{W}{2L}x$	$-\frac{W}{2} + \frac{W}{2L}x$	$\left(1 - \frac{1}{\Theta}\right)\left(\frac{\alpha - \beta}{\Theta} - \frac{1}{\Theta^2} \ln\left(\frac{1 - \beta\Theta}{1 - \alpha\Theta}\right)\right) + \frac{1}{2\Theta}(\beta^2 - \alpha^2)$

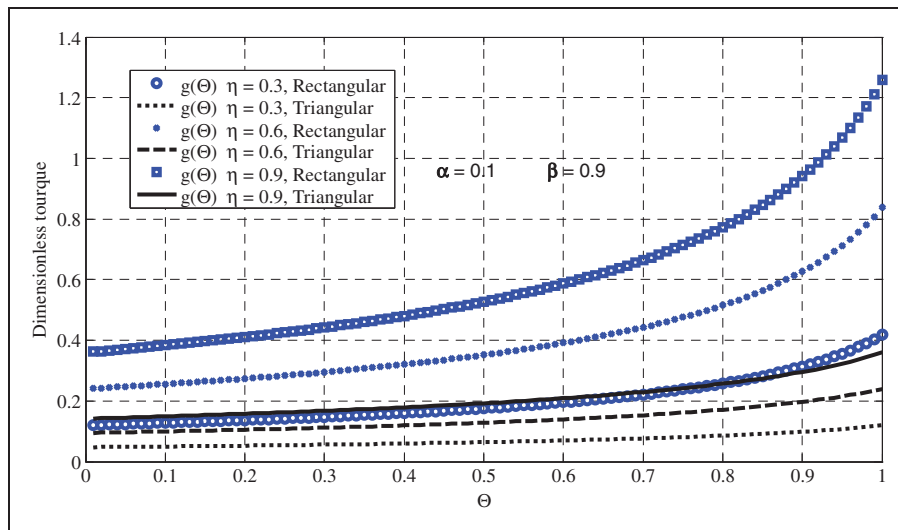


**Figure 2.** Effect of the change of the geometry of the mirror on the dimensionless capillary torque applied to it.

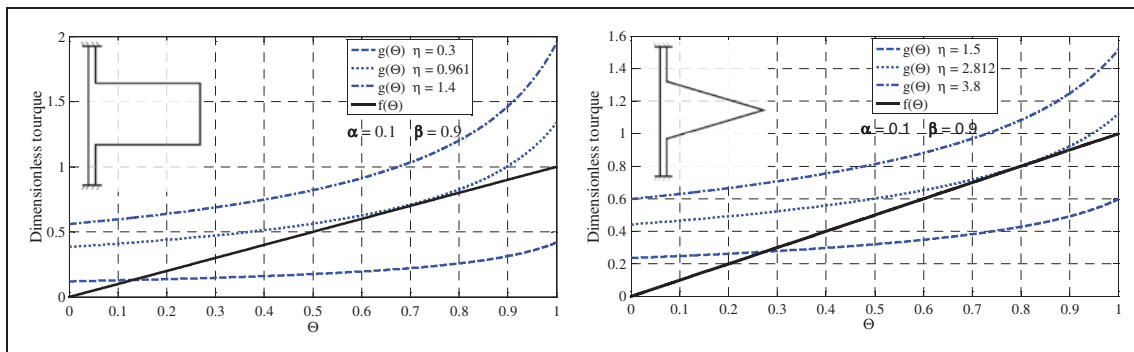


**Figure 3.** Dimensionless elastic restoring torque and capillary torque applied to the different micromirrors.

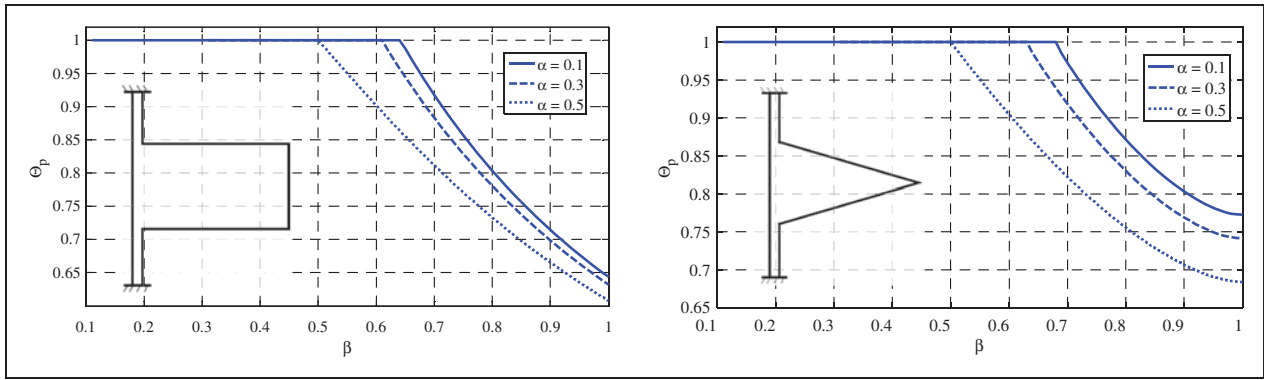


Figure 4.  $\Theta_p$  versus  $\beta$  at various values of  $\alpha$ .

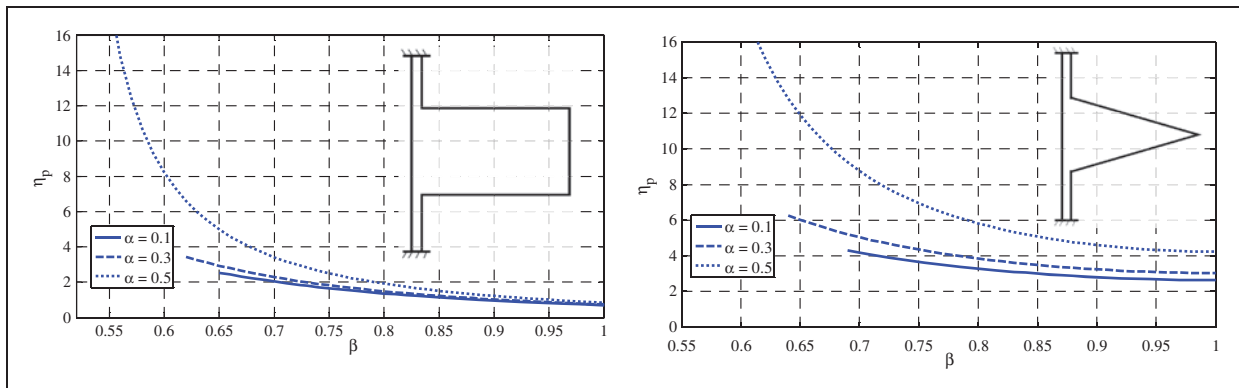


Figure 5.  $\eta_p$  versus  $\beta$  at various values of  $\alpha$ .

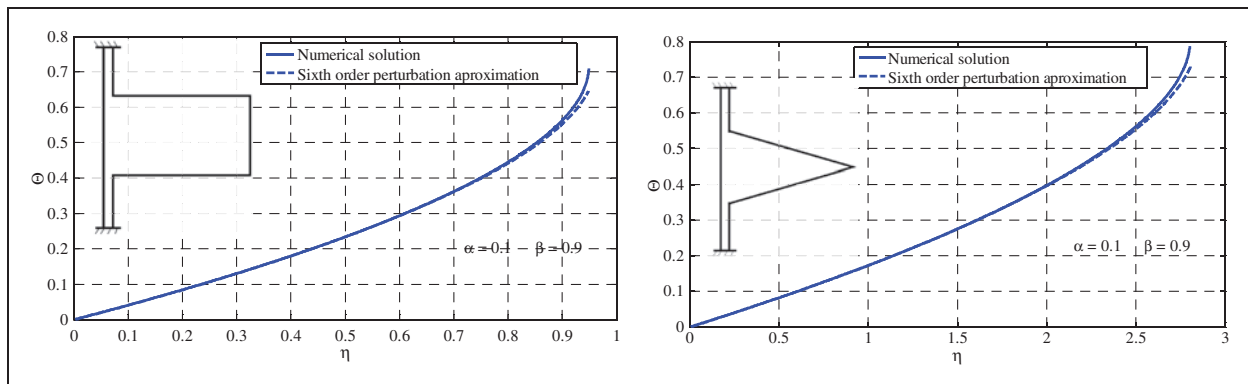


Figure 6. Estimation of micromirror's rotation angles using HPM at  $\alpha = 0.1$  and  $\beta = 0.9$ .

equilibrium point. There exists a certain value of  $\eta$  at which equation (10) has just one root. This value of  $\eta$  is the  $\eta$  at the pull-in state. For  $\eta$  larger than the value of  $\eta$  at pull-in, equation (10) does not have any root and equilibrium cannot be established. So pull-in occurs when  $\eta$  reaches its maximum value at equilibrium

equation, and as a result at pull-in state, equation (15) has to be satisfied

$$\frac{\partial \eta}{\partial \Theta} = 0 \tag{15}$$

By calculating  $\eta$  from equation (10) and substituting it in equation (15), the following equation is obtained for the pull-in angle of the micromirrors under the effect of capillary force

$$\Omega(\Theta_P, \alpha, \beta) = \Theta_P \frac{\partial M(\alpha, \beta, \Theta_P)}{\partial \Theta_P} - M(\alpha, \beta, \Theta_P) = 0 \tag{16}$$

where  $\Omega(\Theta_P, \alpha, \beta)$  is the equation governing the pull-in state of the mirror.

### Pull-in angle

By numerically solving equation (16) for different types of designs of micromirrors presented in Table 1, the pull-in angle of the micromirror can be found versus  $\alpha$  and  $\beta$ . It has to be noted that  $\Theta_P$  is always less than unity and as a result, if the solution of equation (16) leads to  $\Theta_P > 1$ , then it can be concluded that the mirror touches the underneath substrate before the occurrence of pull-in and  $\Theta_P$  would be unity.

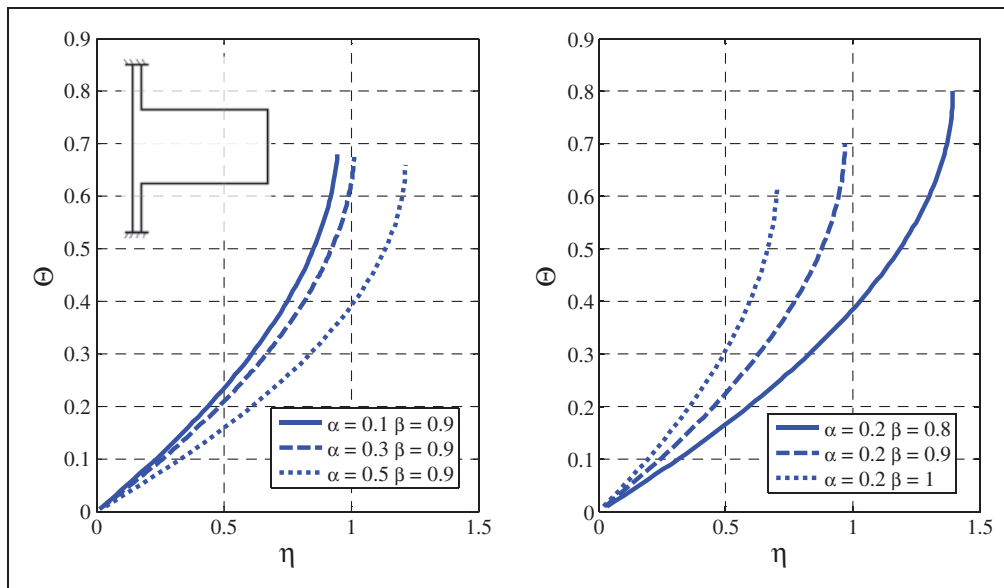


Figure 7. Equilibrium angles of the rectangular mirror versus  $\eta$  for different values of  $\alpha$  and  $\beta$ .

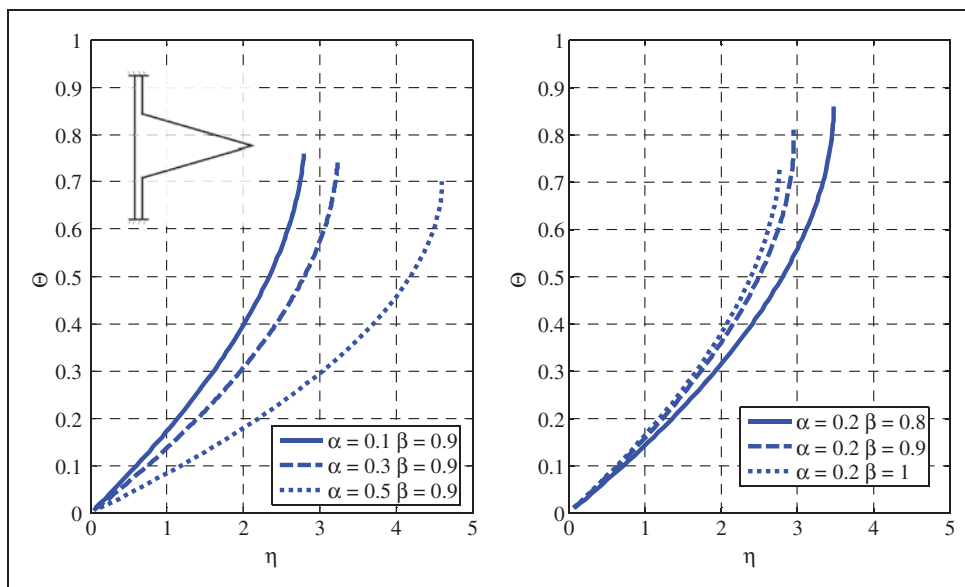


Figure 8. Equilibrium angles of the triangular mirror versus  $\eta$  for different values of  $\alpha$  and  $\beta$ .

In Figure 4,  $\Theta_P$  has been plotted against  $\beta$  at various values of  $\alpha$ . It is observed that with increasing the value of  $\beta$ , the value of  $\Theta_P$  is decreased. It is also observed that at a given value of  $\beta$ , increasing the value of  $\alpha$  would lead to smaller values for  $\Theta_P$ . In other words, the larger the parameters  $a_1$  and  $a_2$  shown in Figure 1, the smaller the pull-in angle of the mirror.

By finding  $\eta$  from equilibrium equation and substituting the respected value of  $\Theta_P$ ,  $\eta_P$ , i.e. the value of  $\eta$  at pull-in is obtained. In Figure 5,  $\eta_P$  is plotted against  $\beta$ . This figure shows that by increasing the

value of  $\beta$  and/or decreasing the value of  $\alpha$ , the value of  $\eta_P$  is decreased. Physically, this sentence means that the smaller the parameter  $a_1$  and/or the larger the parameter  $a_2$ , the larger the torque exerted by capillary forces that results in pull-in.

### Equilibrium behavior of micromirror

In this section, analytical solutions are presented for equilibrium angle of the micromirrors under capillary force. In special cases, the results are compared with numerical FEM results of the commercial FEM software ANSYS.

In order to analytically solve the equilibrium behavior of the mirror, the HPM is utilized. As it was mentioned earlier, this method takes full advantage of the traditional perturbation methods and homotopy techniques. In this method, the unknown parameter is expanded using an embedded parameter which serves as a perturbation parameter. Details of the application of HPM for solving equilibrium equation of micromirrors under capillary force can be found in Appendix 1.

In Figure 6, the results of the numerical simulations are compared with those of analytical HPM results for all types of mirror designs shown in Table 1.

It is observed that the presented closed-form solution for  $\Theta$  closely approximates the numerical solution, especially at low values of  $\eta$ . The accuracy of the presented closed-form solution can be increased with

**Table 2.** Physical properties of the simulated micromirrors.

Parameter	Value
$G$	66 GPa
$\nu$	0.29
$L$	100 $\mu\text{m}$
$W$	100 $\mu\text{m}$
$l$	60 $\mu\text{m}$
$r$	1.5 $\mu\text{m}$
$s$	1.55 $\mu\text{m}$
$\gamma$	$7.2 \times 10^{-2} \text{NM}^{-1}$
$\theta_c$	$5\pi/12$
$a_1$	10 $\mu\text{m}$
$a_2$	90 $\mu\text{m}$

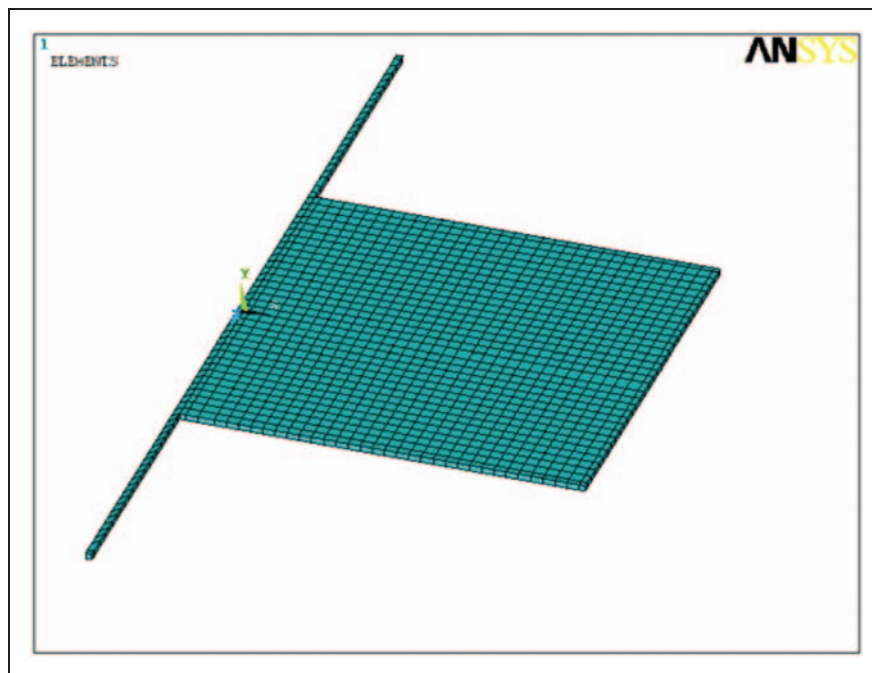


**Figure 9.** Meshed configuration of a rectangular micromirror with characteristics given in Table 2 and with  $h = 56.8 \mu\text{m}$  in ANSYS.

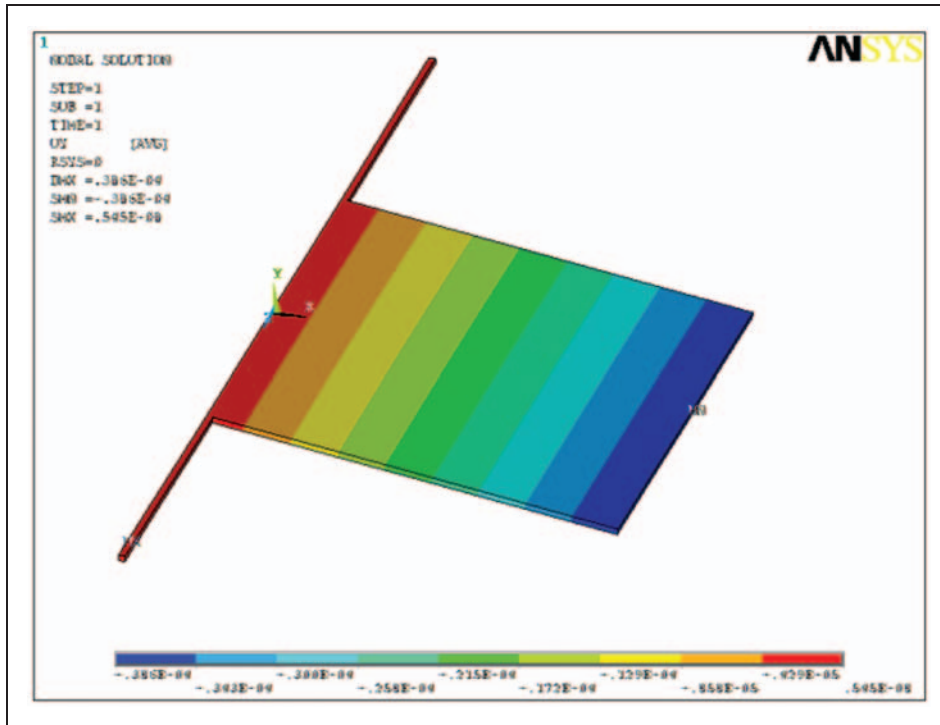


Figure 10. Deformed configuration of the micromirror under capillary force.

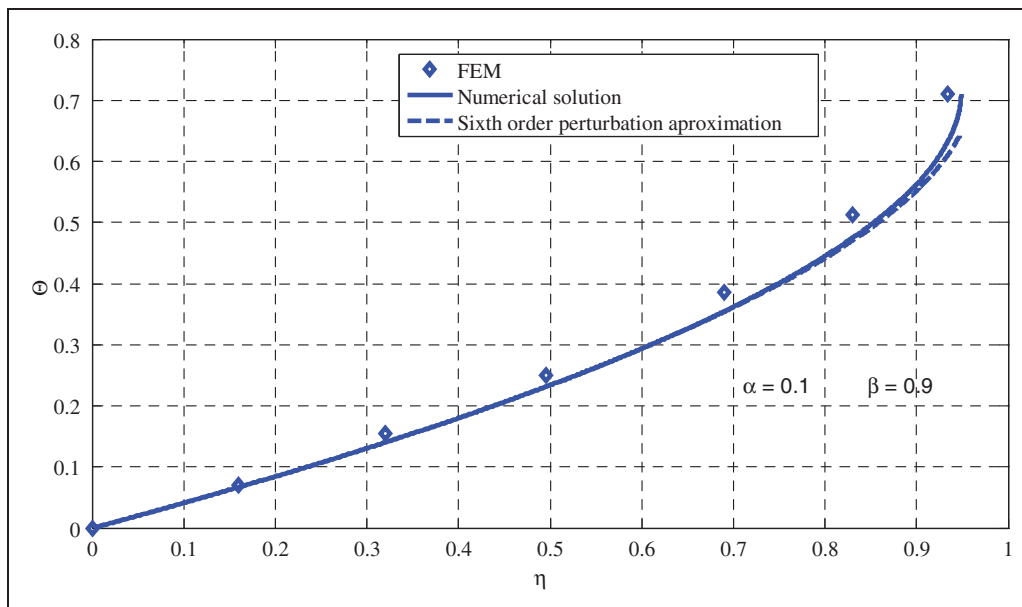


Figure 11. Equilibrium points of the micromirror shown in Figure 10 and properties given in Table 2, and comparison of the FEM results with the results of the numerical model and HPM.

increasing the order of the perturbation expansion used.

In order to investigate the effect of geometrical parameters on mirror’s behavior under capillary force, dimensionless rotation angle  $\Theta$  has been plotted

versus  $\eta$  in Figures 7 and 8 at various values of  $\alpha$  and  $\beta$  for different mirror designs.

From these figures, it is observed that by increasing the value of  $\eta$ , the rotation angle of the micromirror is increased, but the maximum value of  $\eta$  at pull-in,



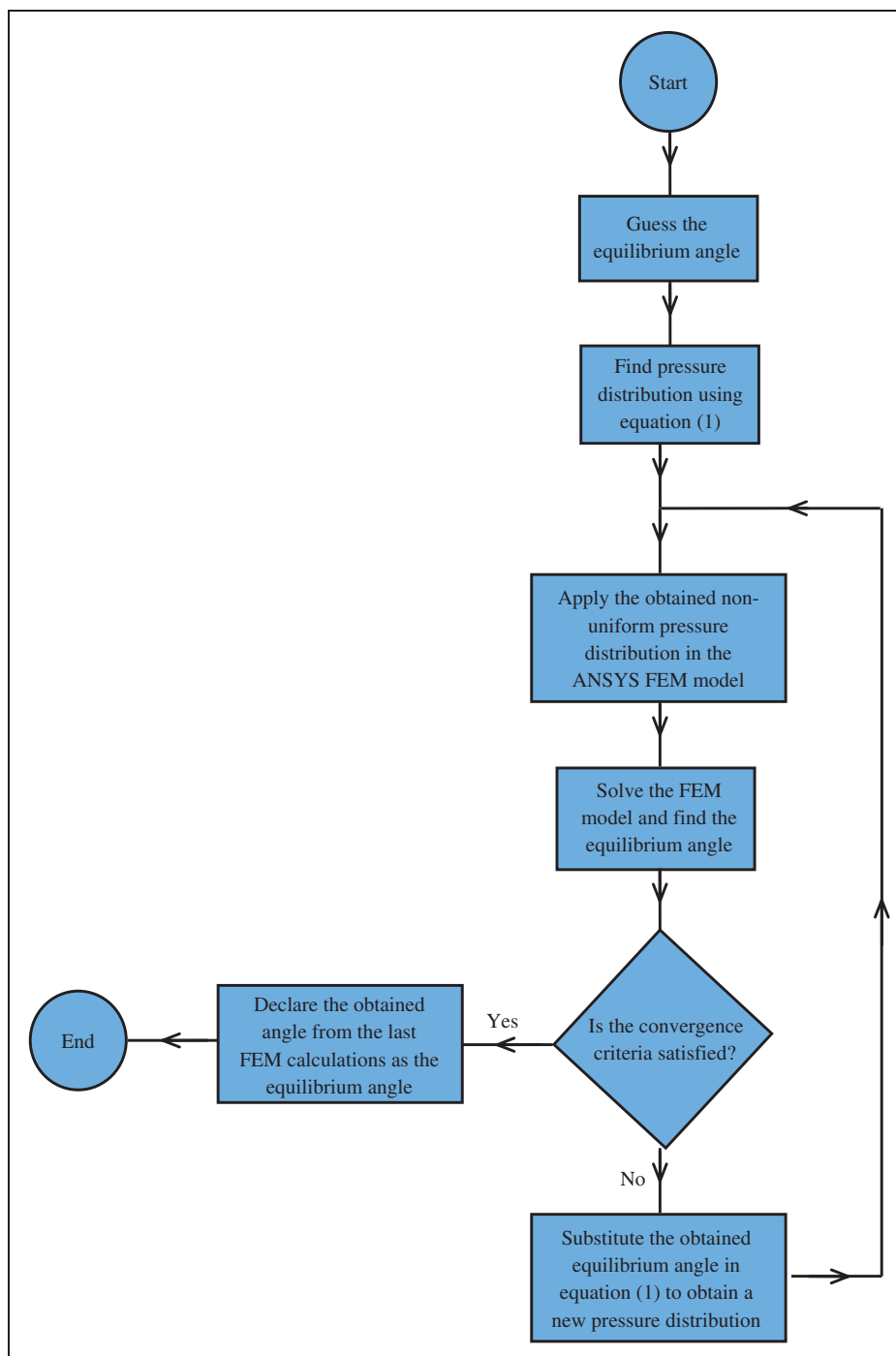


**Figure 12.** The algorithm used for FEM modeling of micromirror under capillary force using the commercial FEM software ANSYS.

strongly depends on the value of  $\beta$  and it is found that by increasing  $\beta$ , the maximum allowable value for  $\eta$  is reduced. Furthermore, it is observed that increasing the value of  $\alpha$ , while keeping  $\beta$  constant would increase the stability limit of the mirror.

In order to verify the accuracy of the presented model, a group of rectangular micromirrors with characteristics given in Table 2 and with different values of  $h$

are simulated using the commercial finite element software ANSYS. The details of modeling the micromirror under capillary force using ANSYS are presented in Appendix 2. Figure 9 shows a sample of this group of micromirrors with  $h = 56.8 \mu\text{m}$  which has been simulated after applying the capillary pressure. In Figure 10, the deflection of the mentioned micromirror under capillary force is depicted. ANSYS output for the

deflection of the mirror has been measured and nondimensionalized to be able to be compared with the results of the presented model in this article. Figure 11 shows that static behavior of micromirrors obtained from the proposed model agrees well with finite element results. This agreement shows that the presented closed-form solution can be used as a fast and accurate design tool for micromirror fabrication.

## Conclusion

The static behavior of micromirrors under the effect of capillary forces was studied. The dimensionless equation governing the static behavior of micromirrors under capillary force was obtained. The pull-in behavior of the mirrors was numerically investigated and the effect of various geometrical parameters was studied. The static behavior of micromirrors was investigated both numerically and analytically using HPM. It was observed that with increasing the instability number, the rotation angle of the micromirror is increased and suddenly the pull-in occurs. A numerical FEM model was also presented to simulate a group of micromirrors and the related results were compared with those of analytical HPM ones. The analytical results were in good agreement with numerical ones.

## Funding

This research received no specific grant from any funding agency in the public, commercial, or not-for-profit sectors.

## Acknowledgments

The authors wish to gratefully acknowledge the nameless reviewers of this article for their useful comments which considerably improved the presenting method and the technical contents of this article.

## References

1. Younis MI. *Modeling and simulation of microelectromechanical systems in multi-physics fields*. PhD Thesis, Virginia Polytechnic Institute and State University, 2004, pp.1–8.
2. Varadan VK, Vinoy KJ and Jose KA. *RF MEMS and their applications*. Chichester, West Sussex: John Wiley & Sons Inc, 2003, pp.2–6.
3. Chao PCP, Chiu CW and Tsai CY. A novel method to predict the pull-in voltage in a closed form for micro-plates actuated by a distributed electrostatic force. *J Micromech Microeng* 2006; 16: 986–998.
4. Hornbeck LJ. Spatial light modulator and method. US Patent 1991, 5,061,049.
5. Ford JE, Aksyuk VA, Bishop DJ, et al. Wavelength add-drop switching using tilting micromirrors. *J Lightwave Technol* 1999; 17: 904–911.
6. Dickensheets DL and Kino GS. Silicon-micromachined scanning confocal optical microscope. *J Microelectromech Syst* 1998; 7(1): 38–47.
7. Zavracky PM, Majumder S and McGruer NE. Micromechanical switches fabricated using nickel surface micromachining. *J Microelectromech Syst* 1997; 6(1): 3–9.
8. Toshiyoshi H and Fujita H. Electrostatic micro torsion mirrors for an optical switch matrix. *J Microelectromech Syst* 1996; 5(4): 231–237.
9. Huang JM, Liu AQ, Deng ZL, et al. An approach to the coupling effect between torsion and bending for electrostatic torsional micromirrors. *Sensors Actuators A* 2004; 115(1): 159–167.
10. Bochobza-Degani O, Elata D and Nemirovsky Y. An efficient DIPIE algorithm for CAD of electrostatically actuated MEMS devices. *J Microelectromech Syst* 2002; 11(5): 612–620.
11. Xiao Z and Farmer KR. Experimental study of micro-machined electrostatic torsion actuators with full travel range. *Sensors Actuators A* 2004; 114: 466–472.
12. Zhang XM, Chau FS, Quan C, et al. A study of the static characteristics of a torsional micromirror. *Sensors Actuators A* 2001; 90: 73–81.
13. Mojahedi M, Moeenfarid H and Ahmadian MT. Analytical solutions for the static instability of nano-switches under the effect of casimir force and electrostatic actuation. In: *Proceedings of the ASME international mechanical engineering congress and exposition*, Lake Buena Vista, FL, USA, 13–19 November 2009, pp.63–69. New York: ASME.
14. Guo JG and Zhao YP. Dynamic stability of electrostatic torsional actuators with van der Waals effect. *Int J Solids Struct* 2006; 43: 675–685.
15. Guo JG and Zhao YP. Influence of van der Waals and Casimir forces on electrostatic torsional actuators. *J Microelectromech Syst* 2004; 13(6): 1027–1035.
16. Gusso A and Delben GJ. Influence of the Casimir force on the pull-in parameters of silicon based electrostatic torsional actuators. *Sensors Actuators A* 2007; 135(2): 792–800.
17. Wei Z and Zhao YP. Growth of liquid bridge in AFM. *J Phys D Appl Phys* 2007; 40(14): 4368–4375.
18. Van Zwol PJ, Palasantzas G and De Hosson JTM. Influence of roughness on capillary forces between hydrophilic surfaces. *Phys Rev E Stat Nonlinear Soft Matter Phys* 2008; 78(3): 031606.
19. Guo JG, Zhou LJ and Zhao YP. Instability analysis of torsional MEMS/NEMS actuators under capillary force. *J Colloid Interf Sci* 2009; 331(2): 458–462.
20. Mastrangelo CH and Hsu CH. Mechanical stability and adhesion of microstructures under capillary forces I. Basic theory. *J Microelectromech Syst* 1993; 2(1): 33–43.
21. Mastrangelo CH and Hsu CH. Mechanical stability and adhesion of microstructures under capillary forces - Part II: Experiments. *J Microelectromech Syst* 1993; 2(1): 44–55.
22. Moeenfarid H, Kahrobaiyan MH and Ahmadian MT. Application of the extended Kantorovich method to the static deflection of microplates under capillary force. In: *Proceedings of the ASME international mechanical engineering congress and exposition*, IMECE2009, Vancouver, British Columbia, Canada, 12–18 November 2009, p.12186. New York: ASME.

23. Zitzler L, Herminghaus S and Mugele F. Capillary forces in tapping mode atomic force microscopy. *Phys Rev B Condens Matter Mater Phys* 2002; 66(15): 1554361–1554368.
24. Li X and Peng Y. Investigation of capillary adhesion between the microcantilever and the substrate with electronic speckle pattern interferometry. *Appl Phys Lett* 2006; 89(23): 234104.
25. Jang J, Schatz GC and Ratner MA. Capillary force in atomic force microscopy. *J Chem Phys* 2004; 120(3): 1157–1160.
26. Younis MI and Nayfeh AH. A study of the nonlinear response of a resonant microbeam to an electric actuation. *Nonlinear Dyn* 2003; 31(1): 91–117.
27. Abdel-Rahman EM and Nayfeh AH. Secondary resonances of electrically actuated resonant microsensors. *J Micromech Microeng* 2003; 13: 491–501.
28. He JH. A coupling method of a homotopy technique and a perturbation technique for non-linear problems. *Int J Non-linear Mech* 2000; 35: 37–43.
29. Moeenfarid H, Mojahedi M and Ahmadian MT. A homotopy perturbation analysis of nonlinear free vibration of Timoshenko microbeams. *J Mech Sci Technol* 2011; 25(3): 279–285.
30. Nayfeh AH. *Introduction to perturbation technique*. New York: John Wiley & Sons Inc, 1993, pp.191–204.

### Appendix I

HPM can be utilized in order to find analytical expressions for  $\Theta$  in equilibrium equation. To do so, equation (10) is divided to a linear and a nonlinear part. Using the Taylor series expansion, the equilibrium equation can be decomposed into a linear  $L(\Theta, \eta, \alpha, \beta)$  and a nonlinear  $N(\Theta, \eta, \alpha, \beta)$  part as follows

$$\Xi(\Theta, \eta, \alpha, \beta) = L(\Theta, \eta, \alpha, \beta) + N(\Theta, \eta, \alpha, \beta) \tag{17}$$

In this equation,  $L(\Theta, \eta, \alpha, \beta)$  and  $N(\Theta, \eta, \alpha, \beta)$  are the linear and nonlinear terms of the Taylor series expansion of  $\Xi(\Theta, \eta, \alpha, \beta)$ , respectively. Obviously,  $N(\Theta, \eta, \alpha, \beta)$  can be obtained by subtracting  $L(\Theta, \eta, \alpha, \beta)$  from  $\Xi(\Theta, \eta, \alpha, \beta)$ . For example, for rectangular micromirrors shown in Table 1,  $L(\Theta, \eta, \alpha, \beta)$  and  $N(\Theta, \eta, \alpha, \beta)$  are obtained as follows

$$L(\Theta, \eta, \alpha, \beta) = -\frac{\eta}{2}(\beta^2 - \alpha^2) + \left(1 - \frac{\eta}{3}(\beta^3 - \alpha^3)\right)\Theta \tag{18}$$

$$N(\Theta, \eta, \alpha, \beta) = \frac{\eta}{\Theta} \left( \beta - \alpha + \frac{1}{\Theta} \ln \left( \frac{1 - \beta\Theta}{1 - \alpha\Theta} \right) \right) + \eta \left( \frac{1}{2}(\beta^2 - \alpha^2) + \frac{1}{3}(\beta^3 - \alpha^3)\Theta \right) \tag{19}$$

Now, the homotopy form is constructed as

$$\mathfrak{S}(\Theta, \eta, \alpha, \beta, P) = L(\Theta, \eta, \alpha, \beta) + P.N(\Theta, \eta, \alpha, \beta) = 0 \tag{20}$$

where  $\mathfrak{S}(\Theta, \eta, \alpha, \beta, P)$  is the homotopy form and  $P$  an embedded parameter. Furthermore,  $\Theta$  is expanded as

$$\Theta = \Theta_0 + P\Theta_1 + P^2\Theta_2 + P^3\Theta_3 + \dots \tag{21}$$

By substituting equation (21) into homotopy form and finding the Taylor series expansion of the resulting

equation with respect to  $P$ , the following equation is obtained

$$\begin{aligned} \mathfrak{S}(\Theta, \eta, \alpha, \beta, P) &= L(\Theta_0, \eta, \alpha, \beta) \\ &+ \left( \Theta_1 \frac{\partial L(\Theta_0, \eta, \alpha, \beta)}{\partial \Theta_0} + N(\Theta_0, \eta, \alpha, \beta) \right) P \\ &+ \left( \Theta_2 \frac{\partial L(\Theta_0, \eta, \alpha, \beta)}{\partial \Theta_0} + \Theta_1 \frac{\partial N(\Theta_0, \eta, \alpha, \beta)}{\partial \Theta_0} \right) P^2 \\ &+ \left( \Theta_3 \frac{\partial L(\Theta_0, \eta, \alpha, \beta)}{\partial \Theta_0} + \Theta_2 \frac{\partial N(\Theta_0, \eta, \alpha, \beta)}{\partial \Theta_0} \right. \\ &\left. + \frac{1}{2} \Theta_1^2 \frac{\partial^2 N(\Theta_0, \eta, \alpha, \beta)}{\partial \Theta_0^2} \right) P^3 + \dots = 0 \end{aligned} \tag{22}$$

By equating coefficient of each power of  $P$  with zero, the following equations are obtained

$$L(\Theta_0, \eta, \alpha, \beta) = 0 \tag{23}$$

$$\Theta_1 \frac{\partial L(\Theta_0, \eta, \alpha, \beta)}{\partial \Theta_0} + N(\Theta_0, \eta, \alpha, \beta) = 0 \tag{24}$$

$$\Theta_2 \frac{\partial L(\Theta_0, \eta, \alpha, \beta)}{\partial \Theta_0} + \Theta_1 \frac{\partial N(\Theta_0, \eta, \alpha, \beta)}{\partial \Theta_0} = 0 \tag{25}$$

$$\begin{aligned} \Theta_3 \frac{\partial L(\Theta_0, \eta, \alpha, \beta)}{\partial \Theta_0} + \Theta_2 \frac{\partial N(\Theta_0, \eta, \alpha, \beta)}{\partial \Theta_0} \\ + \frac{1}{2} \Theta_1^2 \frac{\partial^2 N(\Theta_0, \eta, \alpha, \beta)}{\partial \Theta_0^2} = 0 \end{aligned} \tag{26}$$

Equations (23) to (26) can be iteratively solved for finding  $\Theta_0$ ,  $\Theta_1$ ,  $\Theta_2$ , and  $\Theta_3$ , respectively. Now, according to HPM, by substituting  $P = 1$  and  $\Theta_0$ ,  $\Theta_1$ ,  $\Theta_2$ , and  $\Theta_3$  into equation (21), the value of  $\Theta$  is obtained.

## Appendix 2

In order to model the micromirror's behavior under capillary force using FEM calculations, the geometry of the mirror is modeled in ANSYS and meshed using the SOLID 186 element. The torsion beams supporting the microbeams are considered to be clamped. Since the capillary pressure underneath the mirror is a nonlinear function of the unknown equilibrium angle of the mirror, it is impossible to find and apply the capillary pressure to the mirror in the first step. To overcome this problem, an equilibrium angle is guessed and substituted in equation (1) to find the pressure distribution due to the capillary force. Then, this pressure

distribution is applied to the mirror and the deflection of the mirror and its equilibrium angle is calculated using ANSYS FEM calculations. The obtained equilibrium angle is again used in equation (1) to find a new pressure distribution and this process is continued until it converges to a specific equilibrium angle. In this article, if the change in the equilibrium angle in two consecutive iterates is less than 1%, the problem is considered to have converged. The convergence of the presented procedure is so fast that in most cases two to three iterates are sufficient for finding a precise response. Figure 12 shows the schematic view of the algorithm used for FEM modeling of micromirror under capillary force.